Permanent Magnet Synchronous Machine-Magnetic Lead Screw model based studies on passive and semi-active suspension

A. Stupakowski, A. Højris, M. Pentek, M. Stati, V. Mishukov

Department of Materials and Production, Aalborg University
Fibigerstraede 16, DK-9220 Aalborg East, Denmark
Email: {astupa18, ahajri15, mpente18, mstati18, vmishu18}@student.aau.dk
Web page: http://www.mechman.m-tech.aau.dk/

Abstract

This paper encompasses model based studies on passive and semi-active suspension implemented with a Magnetic Lead Screw (MLS) in combination with Permanent Magnet Synchronous Machine (PMSM). Initially, a brief state of art concerning different suspension schemes is given, leading to an introduction of the PMSM-MLS assembly used as a damping system. Subsequently, the completion of hardware and software controlling the Vehicle Test Platform (VTP) is described. The modelling considerations were narrowed to Quarter Vehicle Model (QVM). The controller design was performed on the linearised PMSM model. As the initial system parameters found through laboratory tests did not represent behaviour of the VTP correctly, new parameters were calculated based on the performed system identification studies from frequency response test. The model with updated parameters was exposed to speed bump test developed in accordance to [1]. The damping force produced by the MLS is calculated from torque, which is linear dependent with the i_q current. The currents are controlled by the PI compensators that equalise the output to the reference and reduce the steady state error. The investigation of damping schemes was limited to model semi-active systems with Skyhook (SH) algorithms and passive suspension. The studies indicate that the use of semi-active systems results in reduction of vertical movement of the chassis and lower energy consumption of PMSM-MLS assembly compared to passive suspension scheme.

Keywords: Permanent Magnet Synchronous Motor, Magnetic Lead Screw, Vehicle Suspension Control, Skyhook, Inverter, Embedded System

1. Introduction

In the recent years, the suspension systems have become a trending research area in the automotive industry. Depending on the principal of operation, there can be distinguished passive, semi-active and active systems.

The passive suspension reduces the motion of the body and wheel by reducing their relative velocities to a rate that gives the required comfort. This is achieved by the use of damping element placed between the chassis and the wheels, such as hydraulic shock absorber [2]. It is the simplest way to protect a vehicle from vibrations and it has proven to be reasonably effective, however due to its passivity, its implementation is always a compromise between resonance control and high frequency isolation [3].

The semi-active systems are based on shock-absorbers with controllable damping coefficients what allows to avoid the trade-off associated with passive systems. They are also known to be cheap to implement and to have low power consumption. Their main limitation is inability to deliver vertical forces in the direction of the suspension velocity. The design of semi-active system is typically made based on SH algorithm. Conceptually, the SH is based on the damper attached between the sprung mass and a fictional reference in the sky. It results that the shock absorber delivers a force proportional purely to the chassis speed rather than the relative velocity between the sprung and unsprung mass [4].

The active systems do not suffer from drawbacks of semi-active systems, as their damping element can generate forces along the direction of the suspension velocity. The method is however associated with large equipment size. Therefore, in the historical view, the research evolved from active to semi-active systems, that have proved to deliver comparable vibrations isolation [5]. The interest of the automotive industry in continuous development of different suspension systems led to intensified research within this field by AAU.

The work has been concentrated on investigating the properties of MLS as a force transmitter. The MLS is inspired by the design of mechanical lead screw consisting of a screw and a nut. The thread is however made of helically shaped magnets. Thereby, when the screw (rotor) is rotated one complete revolution, the nut (translator) translates a certain distance defined by lead γ. The advantage of using magnets is no direct contact resulting in low friction and limited wear while having an efficiency of 90% [6]. This provoked to investigate application of MLS further, that in conjunction with PMSM and an air spring constituted the design of a new shock absorber which can be seen in Fig. 1. The setup allows to generate a damping force independent of suspension velocity and therefore can be used as any type of damper.

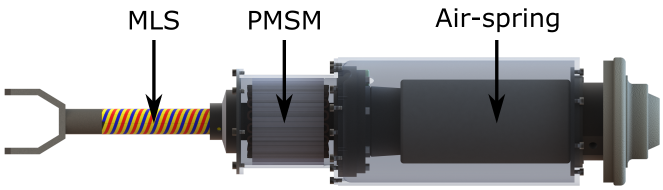

Fig. 1 MLS-PSMS assembly

The PMSM-MLS assembly requires a digital control and therefore, the challenge to be faced in this paper is to implement the passive and the semi-active suspension systems on the microprocessor and to compare their performance characteristic. The research shown in the paper is thus restricted to QVM and aspires to be pre-study for expanding the technology to a complete vehicle model.

The project has been carried out with the use of the VTP developed in [7] consisting of the vehicle with PMSM-MLS assembly and linear transducer. The remaining hardware components were designed in order to complete the prototype consisting of a vehicle with the PMSM-MLS assembly replacing the suspension for one wheel. Depending on the scenario, the PMSM exerts different torque transformed by the MLS into linear damping force. The interconnection between hardware is controlled by the processed sensor's measurements through the microprocessor running with developed software. Subsequently, the model of the test platform was developed and juxtaposed with the physical system. The passive and SH suspension algorithms are modelled and compared to investigate the difference in their behaviour.

2. Method

2.1 Hardware

The completion of hardware setup extends the components of the VTP by additional modules that can be classified as power transmitting elements and sensors. The inverter supplies PMSM with three phase current, which phase magnitudes are measured by dedicated transducers. The inverter's DC-link voltage is measured by a dedicated transducer, what allows to identify if due to the generated back emf, breaking action is needed. The measurements are brought down to values the microprocessor can process by self-designed voltage shifter. It consists of four channels corresponding to each phase and DC-link. The extension of MLS is measured by linear transducer, while the PMSM's angular position and velocity are monitored by the use of a resolver and read by R/D converter. The complete layout of hardware setup with interconnections between elements marked is shown in Fig. 2.

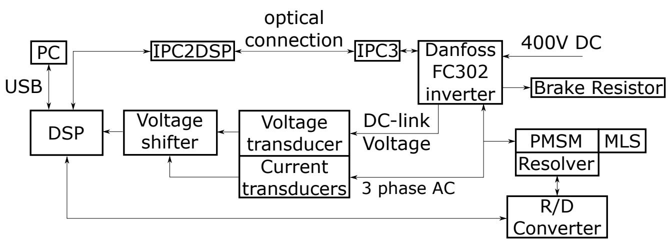

Fig. 2 Hardware layout.

2.2 Software

The interconnection between hardware components is controlled based on the collected and processed measurements through the software implemented on the DSP. The main output from the DSP composes of three PWM signals controlling the IGBTs in the inverter, a PWM signal that enables the breaking resistor to protect the inverter when the PMSM is in generating action.

The PWM signals generation for the inverter is accomplished by the use of three current transducers that feed back the measurements to the controllers. To obtain the average current, the measurements begin when the triangular carrier wave starts counting up what corresponds to the middle point of the high pulse. The currents and DC-voltage are read by ADC module, while the position and velocity are collected through R/D converter and sent via SPI communication protocol. To perform Park transformation, the sine and cosine functions of the electrical angles are found. The phase currents are subsequently transformed into dq-current by Clark and Park transformation schemes and fed to controllers. The dq-voltage requested by the controllers is transformed into PWM signal through inverse transformations and modulated with SVM algorithm, being the chosen modulation scheme.

To ensure trouble less operation of PMSM at high rotational speed, the inverter runs at a frequency of 10 kHz, what also secures low harmonic content in the output [8]. This restricts main code completion time to 100 μs and makes efficient resource management inevitable. Consequently, the trigonometrical functions were replaced with fast approximation Look Up Table with resolution of 360 entries. Each time a trigonometrical operation is needed, function is linearly approximated based on the table content. The resource utilisation for each executed instruction at sampling frequency of 10 kHz is juxtaposed with code loop completion time and can be seen in Fig. 3.

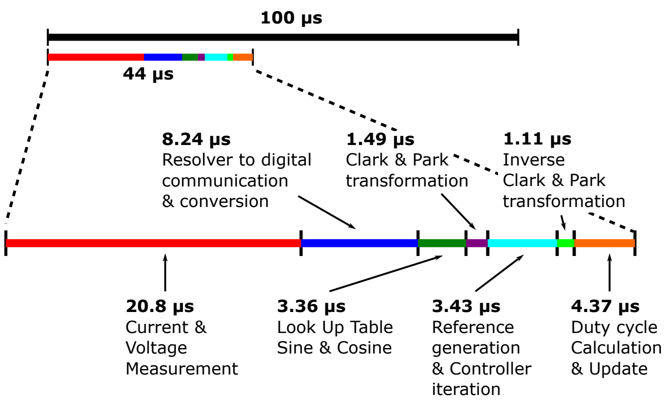

Fig. 3 Resource utilisation of the main code at sampling frequency of 10 kHz.

In order to verify the model, the sensor readings along with controllers inputs and outputs values are being stored in a data table. Accomplishing the operation is succeeded by sending the data to the computer at a low priority to ensure that it does not affect the main functionalities.

2.3 System Modelling

The system behaviour was modelled based on mathematical interpretations of physical phenomena linking the separate components into a single suspension unit. The following section contains methodological description of the modelling procedure for each component.

2.3.1 PMSM

The core foundation of the PMSM is a rotor made of permanent magnets. When the rotor is being rotated a sinusoidal back EMF is generated. To produce a constant torque a constant current is needed on the rotor's q-axis which corresponds to sinusoidal phase currents obtained when the motor rotates. The torque is proportional to the machine constant K_T. The presence of i_d current does not result in any torque and therefore is considered as a loss. The equations were derived in accordance to [9] and can be seen in Eq. 1.

$$
\begin{aligned}
u_d &= R \cdot i_d + L_d \cdot \frac{di_d}{dt} - \omega_E \cdot L_q \cdot i_q \\
u_q &= R \cdot i_q + L_q \cdot \frac{di_q}{dt} + \omega_E \cdot (L_d \cdot i_d + \lambda_{pm}) \\
T_M &= K_T \cdot i_q \\
\ddot{\theta}_M &= \frac{T_M - T_{ext} - B \cdot \dot{\theta}_M}{J}
\end{aligned}
\tag{1}
$$

where:

u_d:	d-axis voltage	i_q:	q-axis current
u_q:	q-axis voltage	L_d:	d-axis inductance
T_M:	Mechanical torque	L_q:	q-axis inductance
T_{ext}:	Load torque	λ_{pm}:	Flux linkage
$\dot{\theta}_M$:	Angular velocity	ω_E:	Electrical speed
$\ddot{\theta}_M$:	Angular acceleration	K_T:	Machine constant
R:	Phase resistance	B:	Damping coefficient
i_d:	d-axis current	J:	Moment of inertia

2.3.2 MLS

The MLS can be viewed as a rotary to transnational gear with a sinusoidal tension spring. Rotating the PMSM's rotor causes the translator to experience linear displacement. Its magnitude is dictated by the lead γ of the MLS. The sinusoidal spring effect is associated with presence of magnets which get misaligned while transferring forces. The magnets are arranged in a Halbach array. The maximum force that can be transmitted is referred to as stall force F_{stall}. Exceeding its value results in braking off the interactions between corresponding magnets and snapping to another position. The schematic of the MLS can be seen in Fig. 4, while the equations used for deriving a mathematical model in Eq. 2.

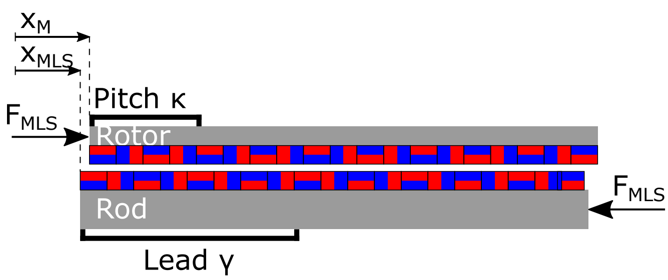

Fig. 4 Principle of MLS With applied load.

$$
\begin{aligned}
x_M &= \frac{\gamma}{2\pi} \cdot \theta_M \\
F_{MLS} &= F_{stall} \cdot sin(\frac{2\pi}{\kappa}(x_M - x_{MLS})) \\
T_{MLS} &= \frac{\gamma}{2\pi} \cdot F_{MLS}
\end{aligned} \tag{2}
$$

where:

x_M:	Rotor offset	θ_M:	Rotor angle
x_{MLS}:	MLS position	T_{MLS}:	MLS torque
F_{MLS}:	MLS force	γ:	Lead
F_{stall}:	Stall force	κ:	Pitch

2.3.3 QVM

The QVM is modelled as a two degree of freedom spring-damper-mass system. The rim, tire, brake and axle constitute the wheel mass being attached to the chassis by a spring, small passive damper due to friction and the MLS. The resilience of the tire is modelled as an additional spring bonding it with the road. The QVM concept is illustrated in Fig. 5. The dynamic equations (Eq. 5) of motion were derived using Lagrange approach.

$$
\begin{aligned}
\ddot{y}_2 =& \frac{1}{m_c}(F_{MLS} - k_1(y_2 - y_1) \\
& - m_c \cdot g - B(\dot{y}_2 - \dot{y}_1)) \\
\ddot{y}_1 =& \frac{1}{m_w}(k_1(y_2 - y_1) - k_2(y_1 - y_0) - F_{MLS} \\
& - m_w \cdot g + B(\dot{y}_2 - \dot{y}_1)) \\
F_n =& - k_2(y_1 - y_0)
\end{aligned} \tag{3}
$$

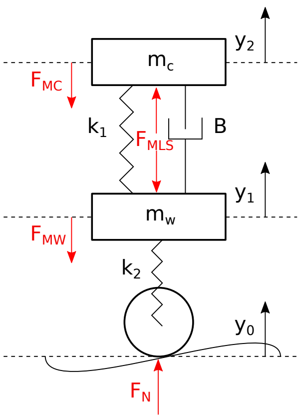

m_c:	Mass of the chassis
m_w:	Mass of the wheel
k_1:	Spring stiffness
k_2:	Tire stiffness
B:	Damping coefficient
y_0:	Road profile
y_1:	Wheel height
y_2:	Chassis height
F_{MC}:	Force due to m_c
F_{MLS}:	MLS force
F_{MW}:	Force due to m_w
F_N:	Normal force

Fig. 5 Quarter vehicle model.

2.4 Linearisation

Due to cross-couplings between u_d-u_q voltages caused by mutual inductance, flux linkage (Eq. 1) and the sinusoidal spring effect in MLS (Eq. 2), the PMSM-MLS assembly show non-linear behaviour. To design the controller, the system was linearised by first order Taylor expansion presented in Eq. 4. The calculations were conducted in accordance to [10].

$$
f(x) = f(x_0) + f'(x_0) \cdot \Delta x \tag{4}
$$

The system was linearised with the assumption, that at average the PMSM-MLS assembly does not move and no torque is needed. The chosen linearisation constants can be seen in Tab. I.

Linearisation constant	Value
I_{d0}	$0\ A$
I_{q0}	$0\ A$
$\dot{\theta}_{M0}$	$0\ rad/s$

Tab. I Point of linearisation.

2.5 Tests

The system parameters were investigated through laboratory tests. This approach allows to maximise the reliability of the model and minimise inaccuracies. The performed studies are described in the following subsections.

2.5.1 Motor parameter tests

Parameters to be determined:

- Phase resistance
- Phase inductance
- Flux-linkage constant
- Iron and friction losses
- Resolver misalignment

a) Phase resistance: The phase resistances were determined by performing a DC-test. The constant DC-voltage with values varying between $0.3 - 1\ V$ was applied to each phase and the corresponding currents measured. The resistances were calculated by the use of Ohm's law and averaged for all collected results.

b) Flux-linkage constant: The flux-linkage was determined by the use of drilling machine mounted to the rotor. The oscilloscope was connected to the phase terminals. The drilling machine was ran with different velocities resulting in voltage induction in the stator windings. The induced line to neutral voltage peak values and frequency spectrum were logged to the oscilloscope. The flux-linkage constant was calculated in accordance with Eq. 5.

$$\lambda_{pm} = \frac{e_{pk}}{f_e \cdot 2\pi} \tag{5}$$

where:

λ_{pm}: Flux-linkage
e_{pk}: Line to neutral voltage peak
f_e: Electrical frequency

c) Phase inductance: On account of surface mounted magnets having a flux-permeability comparable with air, the flux-linkage in the motor is independent on the rotor position. Consequently the L_d and L_q inductance are assumed to be equal. Its magnitude was measured exclusively in the d-axis, which excitation does not result in rotational movement. It was determined by the use of "Wayne Kerr 3260B Precision Magnetics Analyzer" and a "Wayne Kerr 3265B DC Bias Current Unit".

d) Iron and friction losses: The iron and friction losses were found by performing no-load test with keeping the rotor uncoupled from any mechanical load. The balanced three phase voltages were applied to the stator windings at rated frequency and the currents were measured. The test was performed in accordance to procedure described in [11]. The i_q current is directly proportional to the no load torque through machine constant K_T and is equal to the product of viscous friction B_{visc} with rotational velocity ω_M and summed with dry friction forces F_{dry} as shown in Eq. 6. Both the iron and friction losses were considered as viscous friction.

$$i_q \cdot K_T = B_{visc} \cdot \omega_M + F_{dry} \tag{6}$$

e) Alignment test: The test was performed to align the d-axis of PMSM rotor with the resolver readings. The motor was spun what induced phase to neutral back emf which measurements were collected simultaneously with the position from the resolver readings. The offset was found by measuring the difference between the position reading from the resolver with beginning of the sine wave corresponding to the d-axis of the rotor.

2.5.2 Frequency test

The behaviour of the system was validated by the frequency sweep test. The sinusoidal i_q current reference with constant amplitude and varying frequency was used to excite the system. The obtained position responses were used to obtain a frequency spectrum of the system, which subsequently was used to verify the designed controller and the QVM.

2.6 Controllers

The controllers were designed based on the system transfer function, that was derived from the state space representation of the PMSM. The model was derived in accordance to [12] and has a general form of Eq. 7.

$$\begin{aligned} \dot{x} &= Ax + Bu \\ y &= Cx + Du \end{aligned} \tag{7}$$

For the chosen point of linearisation, the Eq. 1 was reduced to the state space form shown in Eq. 8, exclusively connecting the i_d and i_q states to the corresponding u_d and u_q inputs.

$$\begin{aligned} \begin{bmatrix} \dot{i}_d \\ \dot{i}_q \end{bmatrix} &= \begin{bmatrix} -\frac{R}{L} & 0 \\ 0 & -\frac{R}{L} \end{bmatrix} \begin{bmatrix} i_d \\ i_q \end{bmatrix} + \begin{bmatrix} \frac{1}{L} & 0 \\ 0 & \frac{1}{L} \end{bmatrix} \begin{bmatrix} u_d \\ u_q \end{bmatrix} \\ \begin{bmatrix} y_1 \\ y_2 \end{bmatrix} &= \begin{bmatrix} 1 & 0 \\ 0 & 1 \end{bmatrix} \begin{bmatrix} i_d \\ i_q \end{bmatrix} \end{aligned} \tag{8}$$

The resulting system matrix does not include off-diagonal terms and hence is controllable and perfectly decoupled. On account of both states have transfer functions of the same form, the control strategy for u_d-i_d and u_q-i_q voltage-current pairs is the same. Since the i_d current does not produce torque, to minimise losses, its reference is set to 0 value. The torque has a linear dependence with current i_q and therefore the i_{qref} is calculated as a product of torque reference with inverse of machine constant K_T. The control strategy for PMSM-MLS assembly can be seen in Fig. 6.

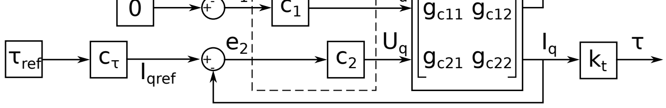

Fig. 6 Control strategy for PMSM-MLS.

The requirements stated for the controllers were chosen based on engineering judgement. They should cancel low frequency disturbances and secure reference tracking ability up to 140% of the resonance frequency of the system measured to be $12Hz$. Since, the u_q-i_q subsystem has a transfer function of the first order the control scheme was completed by PI-controller having a final form of Eq. 9.

$$C(s) = K_p + \frac{K_i}{s} \tag{9}$$

where:

C:	Controller
K_p:	Proportional gain of 0.2337
K_i:	Integrator gain of 1200

The designed controller is frequency dependent and therefore its behaviour after discretisation was analysed. The controller was discretised by Tustin method described in [13] approximating the continuous Laplace operator as in Eq. 10.

$$s \approx \frac{2}{T_s} \frac{z-1}{z+1} \tag{10}$$

where:

T_s: is the sampling time of $\frac{1}{10kHz}$

The closed loop step response of the system with continuous and digital controllers is shown in Fig. 7. The discretisation did not affect the controller's performance.

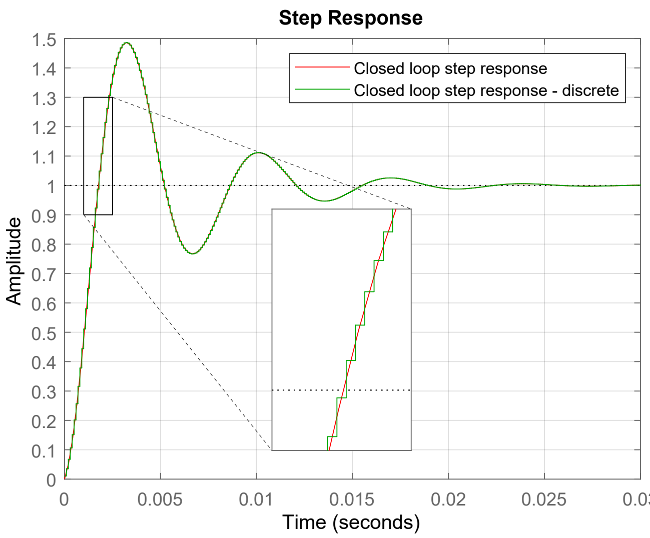

Fig. 7 Closed loop step response for G_{c11}/G_{c22} with continuous and discontinuous controllers.

2.7 Sky hook

The PMSM-MLS can be configured as passive and semi-acitve damper. The passive system can be obtained by calculating the product of relative velocity between the wheel and the chassis with damping factor B_p converting calculations into the torque reference for the motor. Among the semi-active schemes the SH method is best known [4]. It solely acts with regards to the velocity of the chassis to isolate it from vibrations. The difference between the passive and SH concept based semi-active system is shown in Fig. 8.

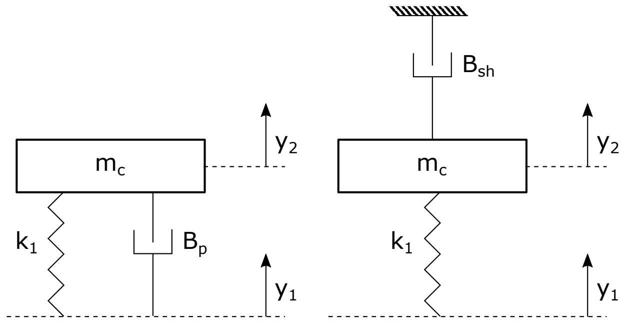

Fig. 8 Passive damper and SH damper scheme

where:

m_c:	mass of the chassis
k_1:	stiffness of the spring
B_p:	damping coefficient for the passive damper
B_{sh}:	damping coefficient for the SH damper
y_1:	vertical position of the wheel
y_2:	vertical position of the chassis

The concept of attaching the damper to a fixed point is purely fictional, however there are two main algorithms for implementation, the linear approximation and its simplification constituted by an on/off control policy [14]. The methods are subsequently presented in Eq. 11 and Eq. 12.

$$B_{sh} = \begin{cases} \dfrac{B_p \cdot \dot{y}_2}{\dot{y}_2 - \dot{y}_1} & \text{if} \quad \dot{y}_2(\dot{y}_2 - \dot{y}_1) > 0, \\ 0 & \text{if} \quad \dot{y}_2(\dot{y}_2 - \dot{y}_1) \leq 0 \end{cases} \tag{11}$$

$$B_{sh} = \begin{cases} B_p & \text{if} \quad \dot{y}_2(\dot{y}_2 - \dot{y}_1) \geq 0, \\ 0 & \text{if} \quad \dot{y}_2(\dot{y}_2 - \dot{y}_1) < 0 \end{cases} \tag{12}$$

Both methods are able to achieve comparable results [3]. To simulate a scenario where the suspension is utilised a speed bump was modelled according to the Danish Road Ministry's guideline [1]. The chosen low-speed sinusoidal bump profile (Modificeret cirkelbump 20 km/h) can be seen in Fig. 9.

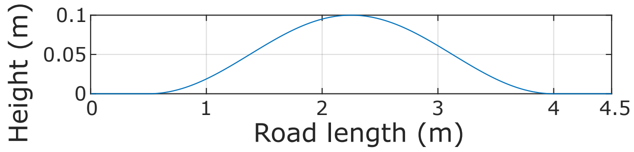

Fig. 9 20 km/h sinusoidal speed-bump profile.

3. Results

This section contains summary of results from performed tests and studies.

3.1 Parameter test

The motor parameters found through laboratory tests can be seen in Tab. II.

Description	Parameter	Value
Flux-linkage	λ_{pm}	0.03 $\frac{Nm}{A}$
Motor Constant	K_t	0.482 $\frac{Nm}{A}$
Inductance	L	1.33 mH
Resistance	R_{LN}	0.339 ohm
Dry Friction	μ_S	0.0654 Nm
Viscous Friction	B_{visc}	0.0017 $\frac{Nm}{rad/s}$
Electrical offset		145°

Tab. II Results from the PMSM parameters & alignment tests.

3.2 Controller test

The performance of the controllers exposed to sinusoidal current input of 3 A with frequency corresponding to resonance behaviour of the VTP is shown in Fig. 10.

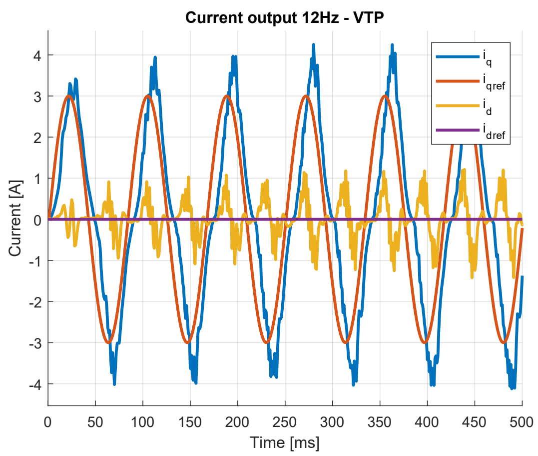

Fig. 10 Reference tracking test of controllers.

The i_d current frequently reaches peaks up to 1.2 A, before it catches the reference, whereas the i_q lags the i_{qref} current by $4 - 10$ ms and has overshoot of $\frac{1}{3}$ of the amplitude.

3.3 Model Verification

The initial verification of the QVM was performed based on the time domain model with estimated QVM parameters. This approach did not result in the model fitting the behaviour of the VTP. Thus the collected frequency spectrum data was used to identify new parameter values in SISO transfer function describing position of the chassis y_L with respect to input force F_{MLS}. The method does not account for non-linear behaviour of the MLS, which was assumed to have ideal gearing ratio. The results of the performed system identification from frequency response studies on the time domain model can be seen in Fig. 11.

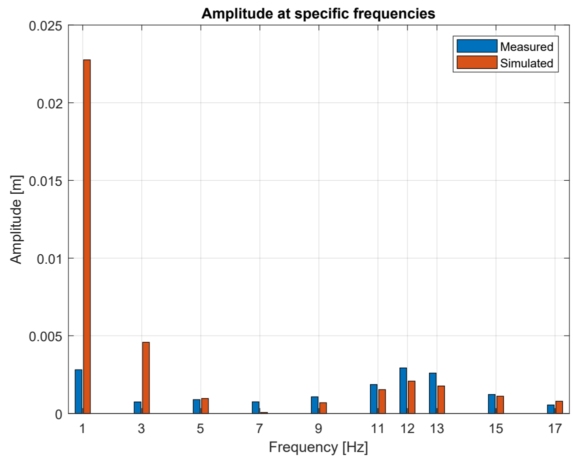

Fig. 11 Frequency spectrum of VTP and the QVM.

The obtained model tends to over-amplify the low frequency inputs. The simulated response is 7.6 and 6 times greater for $1Hz$ and $3Hz$ respectively. The model fits measurements at remaining frequencies.

3.4 Skyhook

The performance of different suspension schemes was validated based on the QVM model derived through frequency response studies. The results given below hold for empirically chosen damping coefficient B_p being $4479.75\ \frac{N \cdot s}{m}$.

The ability of the suspension to restore the relative position y_L between the sprung mass and the wheel exposed to speed bump to its original state can be seen in Fig. 12. The corresponding torques are shown in Fig. 13.

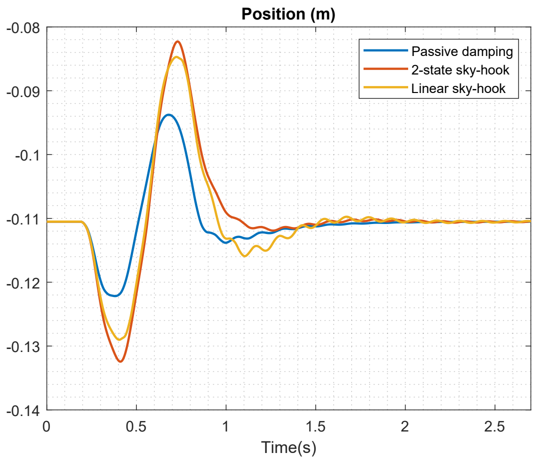

Fig. 12 Relative position y_L under speed bump test.

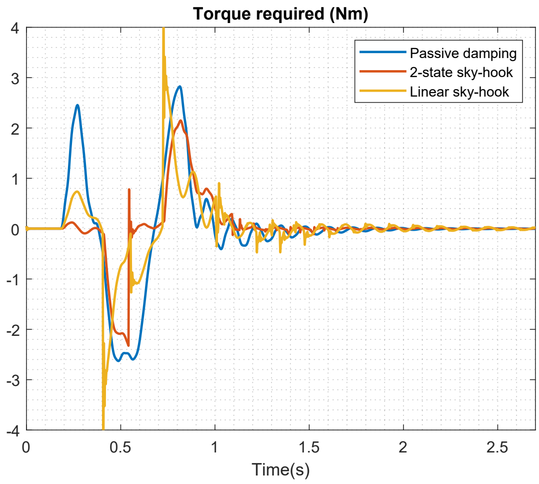

Fig. 13 Torque demands to compensate speed bump oscillations.

The torque requested by linear SH reaches highest extremes, however the values do not compromise functionality of the MLS. The spikes are also shortest observed. The passive scheme noted 40% lower peak which was yet extended in time.

The velocity and acceleration of the chassis are shown in Fig. 14, and in Fig. 15 respectively.

Independent of damping system, the peak velocities reach similar values. The two state SH and the passive system are faster to settle than the linear scheme.

The acceleration in the two state SH has the lowest peaks. The highest peak value is observed in the passive system, however the linear SH needs longest time to settle.

The two-state SH demanded least torque and damped the oscillations first. The work done by each of the

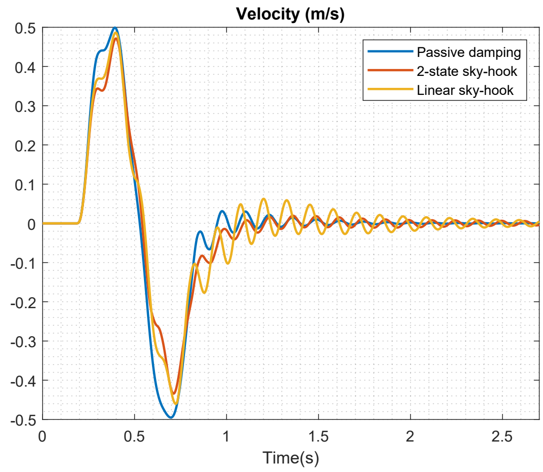

Fig. 14 Velocity of the chassis under speed bump test.

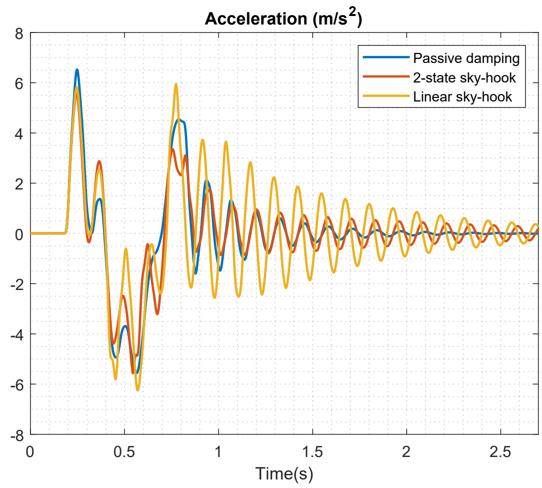

Fig. 15 Acceleration of the chassis under speed bump test.

suspensions schemes was calculated as in Eq. 13 and is summarised in Tab. III.

$$W = \int_{t_0}^{t_{end}} \tau \cdot \omega_M \; dt \tag{13}$$

Suspension scheme	**Value**
Passive	30.84 J
Skyhook - On/Off	19.64 J
Skyhook - Linear	18.73 J

Tab. III Work done to damp oscillations.

The SH methods needed subsequently 36.3% and 39.3% less work to damp all fluctuations than passive scheme.

4. Conclusions

In this paper, to investigate behaviour of passive and semi-active suspension schemes the PMSM-MLS assembly has been incorporated with the established QVM. On account of building an expectation concerning provided drive characteristics, the systems were simulated. The studies show that while the traditional passive damping scheme is capable to provide good overall performance, the SH schemes offer improvements in different areas. The SH schemes manage to reduce the variation in vertical position and velocity of the chassis by allowing the suspension to be compressed more. Furthermore, the two-state SH also lowers the peaks in vertical acceleration of the sprung mass. The SH schemes show reduction in work performed to damp the oscillations, while the two-state SH demands least torque. Consequently, the SH with on/off policy is expected to be the most suitable system among the studied suspension schemes.

Acknowledgement
The authors of this work gratefully acknowledge Grundfos for sponsoring the 7th MechMan symposium.

References

[1] Vejdirektoratet, Katalog over typegodkendte bump. http://www.saferoad.dk/gfx/pdf/pdf08.pdf?fbclid=IwAR3aIA9BvCu4jdFZwfGRaf6asptPQvyEJPDoX4a_u9_ekKRHOEPOExRbFFU, 2013. Downloaded: 07-05-2019.
[2] A. R. Bhise, R. G. Desai, R. N. Yerrawar, A. Mitra, and R. R. Arakerimath, "Comparison between passive and semi-active suspension system using matlab/simulink," IOSR Journal of Mechanical and Civil Engineering, vol. 13, no. 4, pp. 1–6, 2016.
[3] Y. Liu, T. Waters, and M. Brennan, "A comparison of semi-active damping control strategies for vibration isolation of harmonic disturbances," Journal of Sound and Vibration, vol. 280, no. 1, pp. 21 – 39, 2005.
[4] S. M. Savaresi, E. Silani, and S. Bittanti, "Semi-active suspensions: An optimal control strategy for a quarter-car model," IFAC Proceedings Volumes, vol. 37, no. 22, pp. 553 – 558, 2004. IFAC Symposium on Advances in Automotive Control 2004, Salerno, Italy, 19-23 April 2004.
[5] I. Naoki, "Semi-active suspension," KYB Technical Review, vol. 1, no. 55, pp. 31–32, 2017.
[6] R. K. Holm, N. I. Berg, and P. O. Rasmussen, "Theoretical and experimental loss and efficiency studies of a magnetic lead screw," IEEE Transactions on Industry Applications, vol. 51, pp. 1438–1445, 4 2015.
[7] N. I. Berg, "Active suspension - wp1&2. technical report, aalborg university," tech. rep., 2016.
[8] N. Mohan, T. M. Undeland, and W. P. Robbins, Power Electronics Converters, Applicaitons and Design. No. ISBN: 978-81-265-1090-0 in Paperback, John Wiley & Sons Ltd., 2006.
[9] P. Pillay and R. Krishnan, "Modeling of permanent magnet motor drives," IEEE Transactions on Industrial Electronics, vol. 35, no. 4, pp. 537–541, 2004.
[10] C. L. Phillips and J. M. Parr, Feedback Control Systems. Prentice Hall, 5th ed., 2011.
[11] P. C. Sen, Principle of electric machines and power electronics. John Wiley & Sons, 3rd ed., 2014.
[12] S. Skogestad and I. Postlehwaite, Multivariable Feedback Control: Analysis and Design. John Wiley & Sons, 2nd ed., 2005.
[13] T. Wescott, Applied Control Theory of Embedded Systems. No. ISBN: 978-0-7506-7839-1 in Paperback, Elsevier Inc., 2006.
[14] X. Wu and M. Griffin, "A semi-active control policy to reduce the occurrence and severity of end-stop impacts in a suspension seat with an electrorheological fluid damper," Journal of Sound and Vibration, vol. 203, no. 5, pp. 781 – 793, 1997.